



LUND UNIVERSITY

Optical theorem and forward scattering sum rule for periodic structures

Gustafsson, Mats; Vakili, Iman; Bayer Keskin, Sena Esen; Sjöberg, Daniel; Larsson, Christer

2011

[Link to publication](#)

Citation for published version (APA):

Gustafsson, M., Vakili, I., Bayer Keskin, S. E., Sjöberg, D., & Larsson, C. (2011). *Optical theorem and forward scattering sum rule for periodic structures*. (Technical Report LUTEDX/(TEAT-7213)/1-17/(2011); Vol. TEAT-7213). [Publisher information missing].

Total number of authors:

5

General rights

Unless other specific re-use rights are stated the following general rights apply:

Copyright and moral rights for the publications made accessible in the public portal are retained by the authors and/or other copyright owners and it is a condition of accessing publications that users recognise and abide by the legal requirements associated with these rights.

- Users may download and print one copy of any publication from the public portal for the purpose of private study or research.
- You may not further distribute the material or use it for any profit-making activity or commercial gain
- You may freely distribute the URL identifying the publication in the public portal

Read more about Creative commons licenses: <https://creativecommons.org/licenses/>

Take down policy

If you believe that this document breaches copyright please contact us providing details, and we will remove access to the work immediately and investigate your claim.

LUND UNIVERSITY

PO Box 117
221 00 Lund
+46 46-222 00 00

Optical theorem and forward scattering sum rule for periodic structures

Mats Gustafsson, Iman Vakili, Sena E. Bayer, Daniel Sjöberg,
Christer Larsson

Electromagnetic Theory
Department of Electrical and Information Technology
Lund University
Sweden



Mats Gustafsson, Iman Vakili, Daniel Sjöberg
{mats.gustafsson,iman.vakili,daniel.sjoberg}@eit.lth.se

Department of Electrical and Information Technology
Electromagnetic Theory
Lund University
P.O. Box 118
SE-221 00 Lund
Sweden

Sena E. Bayer
senabayer@kocaeli.edu.tr
Sena_Esen.Bayer_Keski@eit.lth.se

Department of Mechatronics Engineering
Kocaeli University
41380 Kocaeli
Turkey

Christer Larsson
Christer.Larsson@saabgroup.com
Christer.Larsson@eit.lth.se

Saab Bofors Dynamics AB
SE-581 88 Linköping
Sweden

Department of Electrical and Information Technology
Electromagnetic Theory
Lund University
P.O. Box 118
SE-221 00 Lund
Sweden

Abstract

Based on energy conservation, an optical theorem is constructed for a slab having an arbitrary periodic microstructure in a plane. A sum rule for low pass structures is derived using analytic properties of Herglotz functions based on causality and passivity. The sum rule relates the extinction cross section to the static polarizability per unit cell, and quantifies the interaction between the slab and electromagnetic fields possible over all wavelengths. The results are illustrated with several numerical and experimental examples.

1 Introduction

The optical theorem relates the forward scattering from an object to the extinction (or total) cross section [22]. It was first discussed more than a century ago by Rayleigh [36] and later extended to quantum mechanics, acoustics, and elastodynamics. There are also formulations of the optical theorem for inhomogeneous backgrounds [19, 20], waveguides [24], corrugated surfaces [39], and in the time domain [16]. The corresponding forward scattering sum rule shows that the extinction cross section integrated over all wavelengths is proportional to the polarizability of the object. It was introduced for dielectric spheroids by Purcell [27] and generalized to arbitrary objects in [6, 34].

The forward scattering sum rule shows that the all-spectrum interaction between the electromagnetic field and an object is proportional to the (static) polarizability of the object. This identity is useful since the solution of a relatively simple static problem provides physical insight in the dynamic scattering over a bandwidth. It also gives physical limitations on the extinction cross section bandwidth product expressed in the polarizability of the object. The sum rule has recently been used to derive an antenna identity and several physical bounds on antennas [7–9, 33]. It has also been used to show bounds on metamaterial scatterers [35] and extraordinary transmission [10].

In this paper, the optical theorem and the forward scattering sum rule are generalized to periodic structures. This version of the optical theorem shows that the extincted power from an incident plane wave is proportional to $\text{Im} h(k)$, where $h(k) = i2(1 - T(k))A$ is a Herglotz function [1], A denotes the cross section area of the unit cell and T the co-polarized part of the lowest order transmission coefficient. The low-frequency asymptotic expansion of $h(k)$ is used to derive the forward scattering sum rule according to the general procedure in [1]. The derivation is solely based on the assumptions that the periodic structure does not support global currents in the low-frequency limit and that the micro structure is made of linear, passive, and time-translational invariant materials.

Moreover, we show that the forward scattering sum rule for isolated objects is retrieved by extending the unit cell length to infinity. An intermediate forward scattering sum rule for two dimensional objects and objects that are periodic in one dimension by letting the unit cell increase in one direction is also derived. The theoretical results are illustrated by numerical simulations and measurements for

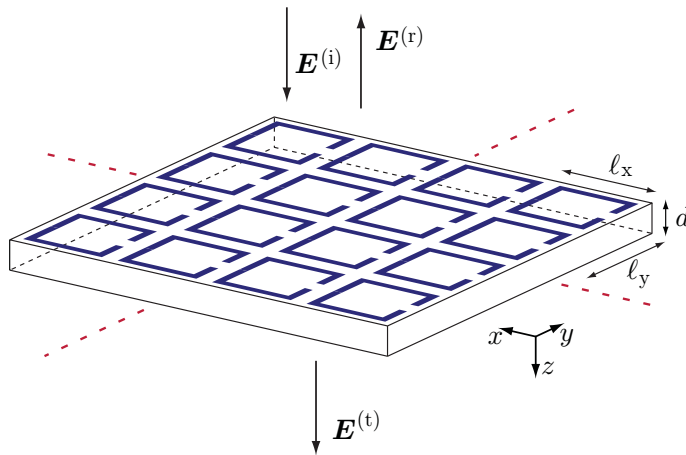


Figure 1: Illustration of a screen with a periodic microstructure. The incident, reflected, and transmitted electric fields are denoted by $\mathbf{E}^{(i)}$, $\mathbf{E}^{(r)}$, and $\mathbf{E}^{(t)}$, respectively. The lattice lengths in the xy -plane are denoted by ℓ_x and ℓ_y , and d is the thickness of the supporting dielectric substrate. The entire structure is assumed to be in the half space $z \leq 0$.

the scattering of a periodic sheet of split ring resonators (SRR) in free space and for a cylinder of SRRs in a parallel plate waveguide.

The new sum rule is instrumental in the understanding of interaction between electromagnetic field and periodic structures with applications for frequency selective surfaces [21], electromagnetic band gap structures [40], and metamaterials [3, 32]. It also provides new insight about the forward scattering sum rule for finite scatterers [6, 34] and its associated antenna identity [8, 9].

This paper is organized as follows. The optical theorem for periodic structures is presented in Sec. 2. A Herglotz function and its high and low-frequency asymptotic expansions are presented in Sec. 3. The forward scattering sum rule is derived in Sec. 4. In Sec. 5, we present numerical and experimental verifications of the sum rule. The paper is concluded in Sec. 6.

2 Optical theorem for periodic structures

We consider a planar periodic structure in otherwise free space. The material and microstructure are modeled with arbitrary linear and temporally dispersive constitutive relations, restricted to causal and passive dispersion models such as, *e.g.*, the Debye, Lorentz, and Drude models [14]. The array is also assumed to not support currents in the low-frequency limit and be sufficiently large to be modeled as an infinite array [12]. This is, *e.g.*, the case for arrays with disjoint metallic inclusions printed on a bulk material with negligible static conductivity.

The array lattice is described by two basis vectors $\ell_x \hat{\mathbf{x}}$ and $\ell_y \hat{\mathbf{y}}$, and the entire heterogeneous structure is contained in the interval $-d \leq z \leq 0$, with a unit cell lying in the xy -plane, see Fig. 1. Consider a time harmonic linearly polarized plane

wave impinging at normal incidence on the array, *i.e.*, $\mathbf{E}^{(i)}(\mathbf{r}) = \mathbf{E}_0 e^{ikz}$, where $\mathbf{E}_0 = E_0 \hat{\mathbf{e}}$, $\hat{\mathbf{e}}$ is a real valued unit vector along the polarization direction of the incident field, $\mathbf{r} = x\hat{\mathbf{x}} + y\hat{\mathbf{y}} + z\hat{\mathbf{z}} = \boldsymbol{\rho} + z\hat{\mathbf{z}}$ is the position vector, k denotes the wavenumber, and time convention $e^{-i\omega t}$ is used.

A spectral decomposition of the transmitted field, $\mathbf{E}^{(t)}$, in Floquet modes is used outside the array

$$\mathbf{E}^{(t)}(k; \mathbf{r}) = \sum_{m=-\infty}^{\infty} \sum_{n=-\infty}^{\infty} \mathbf{E}_{mn}^{(t)}(k) e^{i\mathbf{k}_{mn} \cdot \boldsymbol{\rho}} e^{ik_{z,mn} z}, \quad (2.1)$$

for $z \geq 0$, where $\mathbf{k}_{mn} = m2\pi/\ell_x \hat{\mathbf{x}} + n2\pi/\ell_y \hat{\mathbf{y}}$, and $k_{z,mn} = \sqrt{k^2 - |\mathbf{k}_{mn}|^2}$ is the wavenumber in the z direction for the mn mode. For m or n large enough, $k_{z,mn}$ is an imaginary number indicating an evanescent wave. The expansion coefficients are expressed in the electric field behind the structure as

$$\mathbf{E}_{mn}^{(t)}(k) = \frac{1}{\ell_x \ell_y} \int_{-\ell_y/2}^{\ell_y/2} \int_{-\ell_x/2}^{\ell_x/2} \mathbf{E}^{(t)}(k; x, y, 0) e^{-i\mathbf{k}_{mn} \cdot \boldsymbol{\rho}} dx dy. \quad (2.2)$$

The reflected field, $\mathbf{E}^{(r)}(k; \mathbf{r})$, is similarly expanded in the region $z \leq -d$. The expansion coefficients of the transmitted and reflected fields are related to the incident field via the linear mappings $\mathbf{E}_{mn}^{(t)} = \mathbf{T}_{mn} \cdot \mathbf{E}_0$ and $\mathbf{E}_{mn}^{(r)} = \mathbf{R}_{mn} \cdot \mathbf{E}_0$. It is only a finite number of modes that propagate for a fixed frequency, and, specifically, it is only the zeroth order modes ($m = n = 0$) that propagate for frequencies below the first grating lobe [21], *i.e.*, $f < c_0/\max\{\ell_x, \ell_y\}$. In the following we use the short-hand notation $T = \hat{\mathbf{e}} \cdot \mathbf{T}_{00} \cdot \hat{\mathbf{e}}$ for the co-polarized transmission coefficient T .

We use energy conservation to show an optical theorem for periodic structures, see also [24]. The incident power per unit cell is $P_i = A|E_0|^2/(2\eta_0)$, where $A = \ell_x \ell_y$ is the cross section area of the unit cell. The reflected power, P_r , can be written as a square sum of the expansion coefficients. The corresponding transmitted power, $P_t = |T|^2 P_i + P_{t1}$, is decomposed into the contributions from the co-polarized part of the lowest order mode, $|T|^2 P_i$, and from the remaining modes, P_{t1} . The absorbed power, P_a , is the difference between the incident and the sum of the reflected and transmitted powers, *i.e.*,

$$P_a = P_i - P_r - P_t = P_i - P_r - |T|^2 P_i - P_{t1}. \quad (2.3)$$

The scattered power, P_s , is the sum of the reflected power, P_r , and the power in the scattered part of the transmitted field. This scattered power consists of the power in the co-polarized forward scattered field, *i.e.* the difference between the total field and the incident field, $|1 - T|^2 P_i$, and transmitted power in the remaining modes, P_{t1} , *i.e.*,

$$P_s = P_r + |1 - T|^2 P_i + P_{t1}. \quad (2.4)$$

The extincted power is finally the sum of the absorbed and scattered powers

$$\begin{aligned} P_{\text{ext}} = P_a + P_s &= P_i - P_r - |T|^2 P_i - P_{t1} + P_r + |1 - T|^2 P_i + P_{t1} \\ &= 2 \operatorname{Re}\{1 - T\} P_i \end{aligned} \quad (2.5)$$

that after normalization with the incident power flux, $|E_0|^2/(2\eta_0)$, gives the extinction cross section

$$\sigma_{\text{ext}} = \sigma_a + \sigma_s = 2 \operatorname{Re}\{1 - T\}A. \quad (2.6)$$

This is the optical theorem for the periodic structure. The derivation is based only on energy conservation and the use of a power orthogonal mode decomposition outside the structure, where one mode is singled out and considered fundamental. This calls for two remarks: 1) Since nothing in the derivation changes if we choose an arbitrary Floquet mode \mathbf{E}_{mn} instead of \mathbf{E}_{00} , the optical theorem (2.6) is valid for any Floquet mode. 2) The optical theorem is valid for any structure where a similar mode decomposition can be made, for instance in a waveguiding system.

3 Low- and high-frequency expansions

We use causality and passivity of $T(k)$ to define a Herglotz function that is used to construct sum rules. The transmission coefficient $T(k)$ is holomorphic in k for $\operatorname{Im} k > 0$ due to causality, and bounded in magnitude by unity due to passivity, *i.e.*, $|T| \leq 1$. The logarithm [4, 12, 28], the Cayley transform [5] and many other combinations of T can be used to construct Herglotz functions [1, 11]. Here, we follow the extinction cross section (2.6) and use

$$h(k) = i2(1 - T(k))A \quad (3.1)$$

This is a Herglotz function [1, 25], *i.e.*, $h(k)$ is holomorphic and $\operatorname{Im}\{h(k)\} \geq 0$ for $\operatorname{Im} k > 0$.

It is illustrative to use the mode expansion (2.1) and (2.2) in the free space $z \geq 0$ and express $h(k)$ in the electromagnetic fields. The expansion coefficients (2.2) simplify for the transmission coefficient, which is given by the average of the electric field behind the structure. This gives the explicit expression

$$\begin{aligned} h(k) &= i2 \left(1 - \frac{\hat{\mathbf{e}} \cdot \mathbf{E}_{00}^{(t)}(k)}{E_0} \right) \ell_x \ell_y = \frac{-2i}{E_0} \int_{-\ell_y/2}^{\ell_y/2} \int_{-\ell_x/2}^{\ell_x/2} \hat{\mathbf{e}} \cdot \mathbf{E}^{(s)}(k; x, y, 0) \, dx \, dy \\ &= \frac{-i}{E_0} \int_{-\ell_y/2}^{\ell_y/2} \int_{-\ell_x/2}^{\ell_x/2} \hat{\mathbf{e}} \cdot \mathbf{E}^{(s)}(k; x, y, 0) + \eta_0(\hat{\mathbf{z}} \times \hat{\mathbf{e}}) \cdot \mathbf{H}^{(s)}(k; x, y, 0) \, dx \, dy, \end{aligned} \quad (3.2)$$

where the scattered field $\mathbf{E}^{(s)} = \mathbf{E}^{(t)} - \mathbf{E}^{(i)}$ is used. The last line is obtained by using the fact that the zeroth order modes are plane waves propagating in the positive z direction, and all higher modes integrate to zero.

For a low-pass structure, the low-frequency asymptote of T is obtained from the Maxwell equations by an expansion of the fields in powers of k as discussed in [12, 17, 30], *i.e.*,

$$h(k) \sim k\gamma = k(\hat{\mathbf{e}} \cdot \boldsymbol{\gamma}_e \cdot \hat{\mathbf{e}} + (\hat{\mathbf{k}} \times \hat{\mathbf{e}}) \cdot \boldsymbol{\gamma}_m \cdot (\hat{\mathbf{k}} \times \hat{\mathbf{e}})) \quad (3.3)$$

as $k \rightarrow 0$. The electric and magnetic static polarizabilities $\boldsymbol{\gamma}_e$ and $\boldsymbol{\gamma}_m$ provide the induced electric and magnetic dipole moments per unit cell, $\mathbf{p} = \epsilon_0 \boldsymbol{\gamma}_e \cdot \mathbf{E}$ and

$\mathbf{m} = \boldsymbol{\gamma}_m \cdot \mathbf{H}$, when the structure is subjected to constant electric and magnetic fields \mathbf{E} and \mathbf{H} , respectively. More precisely, $\boldsymbol{\gamma}_e$ is defined as [34, 35]

$$\hat{\mathbf{e}} \cdot \boldsymbol{\gamma}_e \cdot \hat{\mathbf{e}} = \frac{1}{E_0} \int_{\Omega \times [-d, 0]} \hat{\mathbf{e}} \cdot (\boldsymbol{\epsilon}(0; \mathbf{r})/\epsilon_0 - \mathbf{I}) \cdot \mathbf{E}(0; \mathbf{r}) \, dV, \quad (3.4)$$

where the zero-frequency field $\mathbf{E}(0; \mathbf{r})$ has the prescribed mean value $\hat{\mathbf{e}}$ and satisfies the electrostatic equations

$$\nabla \times \mathbf{E}(0; \mathbf{r}) = \mathbf{0}, \quad \nabla \cdot (\boldsymbol{\epsilon}(0; \mathbf{r}) \cdot \mathbf{E}(0; \mathbf{r})) = 0, \quad (3.5)$$

in the unit cell $\Omega \times \mathbb{R}$, with periodic boundary conditions in the xy -plane. Here, $\boldsymbol{\epsilon}(0; \mathbf{r})$ is the static permittivity dyadic (which is real-valued, symmetric, and positive-definite), and ϵ_0 is the free space permittivity. This system of partial differential equations can be solved using the Finite Element Method, typically by representing the electric field with a scalar potential as $\mathbf{E}(0; \mathbf{r}) = \hat{\mathbf{e}}E_0 - \nabla\varphi(\mathbf{r})$ and solving the elliptic equation $\nabla \cdot [\boldsymbol{\epsilon} \cdot (\hat{\mathbf{e}}E_0 - \nabla\varphi)] = 0$, where the scalar potential φ is periodic in the plane and decays to zero as $z \rightarrow \pm\infty$ if $\hat{\mathbf{e}}$ is in the plane. The elliptic nature of the problem means this numerical solution provides an upper bound to the polarizability; solving the problem with a vector potential instead provides a lower bound [31]. Integral equation solvers such as the method of moments (MoM) are sometimes preferred, particularly due to their efficiency in model problems involving only metal structures and no materials.

The static problem (3.5) possesses some variational properties, which can be used to show that the polarizability dyadic is monotone in $\boldsymbol{\epsilon}$ in the respect that if $\boldsymbol{\epsilon}$ is increased anywhere in $\Omega \times [-d, 0]$, then the quadratic form $\hat{\mathbf{e}} \cdot \boldsymbol{\gamma}_e \cdot \hat{\mathbf{e}}$ (simply referred to as the polarizability throughout this paper) does not decrease [15, 31]. The magnetic polarizability dyadic, $\boldsymbol{\gamma}_m$, is defined analogously, by substituting $(\mathbf{E}, \boldsymbol{\epsilon}) \rightarrow (\mathbf{H}, \boldsymbol{\mu})$.

The high-frequency asymptotic is $h(k) = \mathcal{O}(1)$ as $k \hat{\rightarrow} \infty$, where $\hat{\rightarrow}$ denotes limits taken inside the upper half complex plane. This follows from passivity $|T(k)| \leq 1$ and hence $|h(k)| \leq 4A$ for all k .

4 Forward scattering sum rules

Sum rules are equations stating that the sum or integral of a certain quantity has a given value. In particular, a large variety of sum rules can be derived for Herglotz functions [1], where typically the integrand is the imaginary part of the Herglotz function weighted by some function of frequency k , and the integral is related to the low- and high frequency expansions of the function. In the present case where the Herglotz function is given by the extinction cross section (3.1), the asymptotic expansions are

$$h(k) \sim \begin{cases} k\gamma & \text{as } k \hat{\rightarrow} 0 \\ \mathcal{O}(1) & \text{as } k \hat{\rightarrow} \infty \end{cases} \quad (4.1)$$

and the relevant sum rule is [1]

$$\frac{2}{\pi} \int_0^\infty \frac{\sigma_{\text{ext}}(k; \hat{\mathbf{k}}, \hat{\mathbf{e}})}{k^2} \, dk = \hat{\mathbf{e}} \cdot \boldsymbol{\gamma}_e \cdot \hat{\mathbf{e}} + (\hat{\mathbf{k}} \times \hat{\mathbf{e}}) \cdot \boldsymbol{\gamma}_m \cdot (\hat{\mathbf{k}} \times \hat{\mathbf{e}}), \quad (4.2)$$

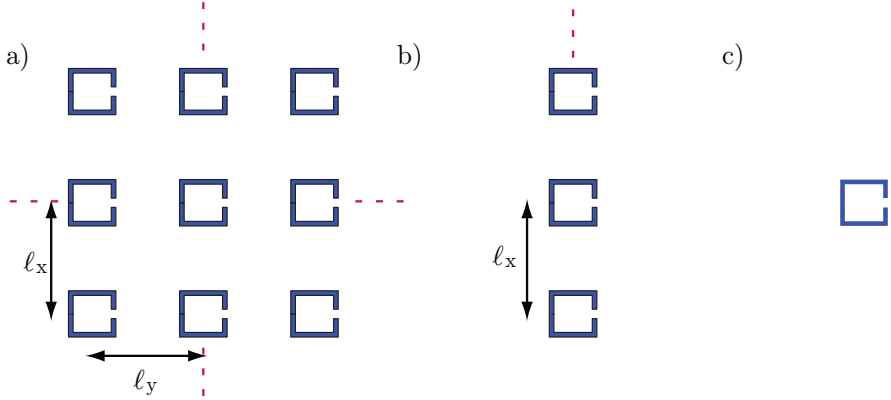


Figure 2: Scattering geometries. a) periodic in two directions. b) periodic in one direction. c) single object.

where $\sigma_{\text{ext}} = \text{Im } h$ is used. It is convenient to rewrite the sum rule in the wavelength variable, $\lambda = 2\pi/k$, that transforms (4.2) into

$$\frac{1}{\pi^2} \int_0^\infty \sigma_{\text{ext}}(\lambda; \hat{\mathbf{k}}, \hat{\mathbf{e}}) d\lambda = \hat{\mathbf{e}} \cdot \boldsymbol{\gamma}_e \cdot \hat{\mathbf{e}} + (\hat{\mathbf{k}} \times \hat{\mathbf{e}}) \cdot \boldsymbol{\gamma}_m \cdot (\hat{\mathbf{k}} \times \hat{\mathbf{e}}), \quad (4.3)$$

where the symbol $\sigma_{\text{ext}}(k; \hat{\mathbf{k}}, \hat{\mathbf{e}})$ is reused as the extinction cross section as a function of the wavelength. We observe that (4.2) is identical to the forward scattering sum rule with σ_{ext} being the extinction cross section for an object in free space [6, 34]. The identity (4.3) is bounded to derive a physical limitation on the product between the bandwidth and extinction cross section

$$\frac{\lambda_2 - \lambda_1}{\pi^2} \min_{\lambda \in [\lambda_1, \lambda_2]} \sigma_{\text{ext}}(\lambda) \leq \hat{\mathbf{e}} \cdot \boldsymbol{\gamma}_e \cdot \hat{\mathbf{e}} + (\hat{\mathbf{k}} \times \hat{\mathbf{e}}) \cdot \boldsymbol{\gamma}_m \cdot (\hat{\mathbf{k}} \times \hat{\mathbf{e}}). \quad (4.4)$$

The sum rule is valid for arbitrary periodic structures that do not support currents in the static limit and is composed by linear and passive materials. In the following, we show that the forward scattering sum rule [6, 34] for isolated objects is obtained by extending the unit cell in two directions, *i.e.*, by letting $\ell_x = \ell_y \rightarrow \infty$, see Fig. 2c. We also obtain an intermediate sum rule for two-dimensional objects and for objects that are periodic in one direction, see Fig. 2b.

As $\ell_x = \ell_y = \ell \rightarrow \infty$, the low-frequency limit is obtained by replacing Ω with \mathbb{R}^2 in (3.4) and (3.5) and observing that the potential $\varphi(\mathbf{r})$ vanish as $|\mathbf{r}| \rightarrow \infty$. The decay of the potential follows from the expression of the potential as a sum over the induced dipole moments, *i.e.*,

$$\varphi(\mathbf{r}) = \sum_{m=-\infty}^{\infty} \sum_{n=-\infty}^{\infty} \frac{\mathbf{r} - \mathbf{r}_{mn}}{4\pi|\mathbf{r} - \mathbf{r}_{mn}|^3} \cdot \boldsymbol{\gamma}_e \cdot \mathbf{E}_0 \quad (4.5)$$

where $\mathbf{r}_{mn} = m\ell_x \hat{\mathbf{x}} + n\ell_y \hat{\mathbf{y}} + \zeta \hat{\mathbf{z}}$. Note, that the monopole term vanishes as the objects are uncharged. The sum is convergent for $\mathbf{r} \neq \mathbf{r}_{mn}$ and it shows that the potential

between the objects decay, *e.g.*, for $\mathbf{r} = \mathbf{r}_{11}/2$, to zero as $\ell \rightarrow \infty$. The polarizability dyadic γ_e approximates hence the free space polarizability dyadic [17, 34] as $\ell \rightarrow \infty$.

The entire periodic structure contributes to the scattered field for a finite unit cell. However, the contributions from the neighboring objects decrease as $\ell \rightarrow \infty$. The integral representation (3.2) is used to express h in the fields behind the structure as

$$h(k) \rightarrow h_3(k) = \frac{-i}{E_0} \int_{\mathbb{R}^2} \hat{\mathbf{e}} \cdot \mathbf{E}^{(s)}(k; x, y, 0) + \eta_0(\hat{\mathbf{z}} \times \hat{\mathbf{e}}) \cdot \mathbf{H}^{(s)}(k; x, y, 0) dx dy \quad (4.6)$$

in the limit $\ell \rightarrow \infty$. The right-hand side of (4.6) is recognized as the surface integral representation of the electromagnetic field expressing the far field in the scattered field on the surface $z = 0$, *i.e.*, $h_3(k) = 4\pi \lim_{z \rightarrow \infty} z e^{-ikz} \hat{\mathbf{e}} \cdot \mathbf{E}^{(s)}(k, z\hat{\mathbf{z}})/(kE_0)$, see [6]. This shows that $\text{Im } h_3(k) = \sigma_{\text{ext}}(k)$, where σ_{ext} denotes the extinction cross section for an object in free space. This forward scattering sum rule has been extensively verified [6, 34, 35] and is useful in the analysis of small antennas [8, 9].

The case with $\ell_y \rightarrow \infty$ corresponds to a situation with periodicity in the x -direction, see Fig. 2b. This scattering configuration is found in scattering of elongated objects that can be approximated by two dimensional scattering. Following the analysis above, we let $\ell_y \rightarrow \infty$ in (3.2), to get the Herglotz function

$$\begin{aligned} h(k) &= i2\ell_x \ell_y (1 - T(k)) \rightarrow h_2(k) \ell_x \\ &= \frac{-i}{E_0} \int_{\mathbb{R}} \int_{-\ell_x/2}^{\ell_x/2} \hat{\mathbf{e}} \cdot \mathbf{E}^{(s)}(k; x, y, 0) + \eta_0(\hat{\mathbf{z}} \times \hat{\mathbf{e}}) \cdot \mathbf{H}^{(s)}(k; x, y, 0) dx dy \quad (4.7) \end{aligned}$$

After dividing with ℓ_x , we recognize the first term in the right-hand side of (4.7) as the mean electric field on the line described by $z = 0$ and $-\infty < y < \infty$, and correspondingly for the magnetic field. The right hand side is then seen to be the line integral representation of the electromagnetic field expressing the 2D far field in the scattered field at $z = 0$, *i.e.*, $h_2(k) = \lim_{z \rightarrow \infty} (i8\pi k z)^{1/2} e^{-ikz} \hat{\mathbf{e}} \cdot \mathbf{E}^{(s)}(k, z\hat{\mathbf{z}})/(kE_0)$, see [2, p. 6] and [29, p. 207]. This shows that $\text{Im } h_2(k) = \sigma_{\text{ext},2\text{D}}(k)$, where $\sigma_{\text{ext},2\text{D}}$ denotes the extinction cross section per unit length of an infinite cylindrical object.

5 Examples

We demonstrate the sum rule (4.3) in four applications: transmission through dielectric slabs, arrays of lossy split ring resonators, perfectly conducting split ring resonators on a dielectric substrate, and a resonant cylinder structure.

5.1 Dielectric slabs

The transmission and reflection coefficients of a homogeneous isotropic slab with thickness d are

$$T = \frac{(1 - r_0^2)e^{i(n-1)kd}}{1 - r_0^2 e^{2inkd}} \quad \text{and} \quad R = r_0 \frac{1 - e^{2inkd}}{1 - r_0^2 e^{2inkd}}, \quad (5.1)$$

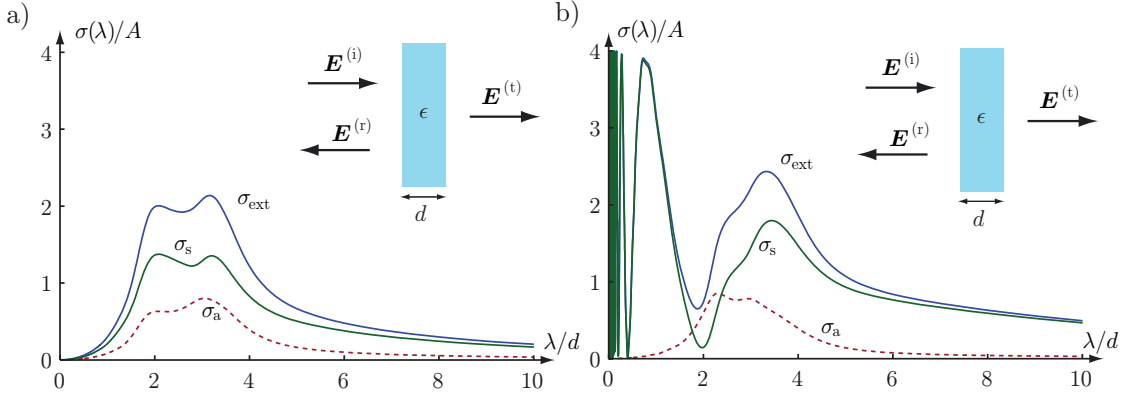


Figure 3: Simulated values for the absorption σ_a , scattering σ_s , and extinction σ_{ext} cross sections of dielectric slabs with the Lorentz models $\epsilon_r(k) = 1 + 1/(1 - i0.1k - 0.2k^2)$ and $\epsilon_r(k) = 2 + 1/(1 - i0.1k - 0.2k^2)$ in a) and b), respectively.

respectively, where $n = \sqrt{\epsilon_r \mu_r}$ is the refractive index, $r_0 = (1 - \eta_r)/(1 + \eta_r)$, and $\eta_r = \sqrt{\mu_r/\epsilon_r}$ is the relative impedance. The generalized scattering, absorption, and extinction cross sections are $\sigma_s = A(|R|^2 + |1 - T|^2)$, $\sigma_a = A(1 - |R|^2 - |T|^2)$, and $\sigma_{\text{ext}} = 2A \text{Re}\{1 - T\}$, respectively, see also the optical theorem (2.6).

Consider a dielectric slab with thickness $d = 1$ and the permittivity modeled by the Lorentz model $\epsilon_r(k) = \epsilon_\infty + (\epsilon_s - \epsilon_\infty)/(1 - 0.1ik - 0.2k^2)$, where d and k are dimensionless quantities. The absorption, scattering, and extinction cross sections are depicted in Fig. 3 for $\{\epsilon_\infty = 1, \epsilon_s = 2\}$ and $\{\epsilon_\infty = 2, \epsilon_s = 3\}$. The left hand sides of the sum rule (4.3) are determined numerically to A and $2A$. This agrees with the polarizability $(\epsilon_s - 1)dA$ and confirms the sum rule (4.3). Note the oscillations at low λ/d for the case $\{\epsilon_\infty = 2, \epsilon_s = 3\}$, corresponding to the positive insertion delay with respect to the background in the high-frequency limit for this case.

An experimental demonstration is obtained as follows. Transmission is measured from 20 MHz to 20 GHz using an Agilent E8363B network analyzer and a coaxial fixture with length 50.81 mm, and inner and outer diameters of 3.05 mm and 6.97 mm, respectively. Two material samples filling the cross section are used, having lengths $d_1 = 9.11$ mm and $d_2 = 8.94$ mm, and relative permittivities $\epsilon_{1r} \approx 2.1 + 0.01i$ and $\epsilon_{2r} \approx 2.7 + 0.02i$ almost constant throughout the band, respectively. The transmission coefficient T is calculated as the insertion loss S_{21} for the fixture with a sample present normalized by the insertion loss for the empty fixture, $T = S_{21}^{(\text{sample})}/S_{21}^{(\text{empty})}$.

Two different configurations are investigated: 1) with the two dielectric samples adjacent to each other, and 2) separated by a distance of 8.77 mm. These two configurations are chosen since they have the same static polarizability per unit area, $\gamma/A = (\epsilon_{1r} - 1)d_1 + (\epsilon_{2r} - 1)d_2$, but different frequency dependence due to their different geometric structure. The polarizability for each case is calculated from measurement data by determining the effective permittivity for the two configurations using the Nicolson-Ross-Weir algorithm [23, 38] at 20 MHz, and using $\gamma = (\text{Re}(\epsilon_{\text{eff}}) - 1)Ad$.

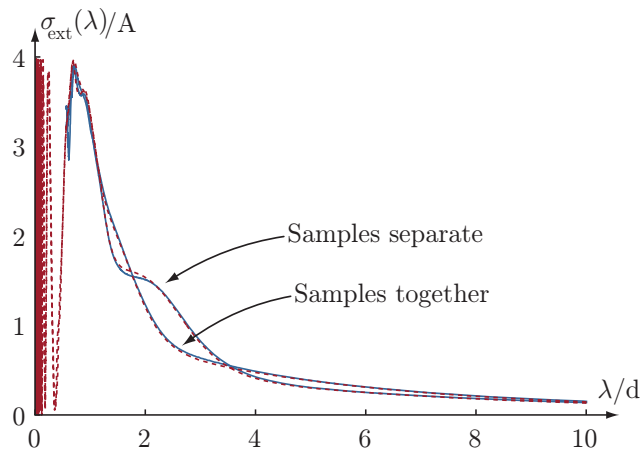


Figure 4: Measured values (solid curves) and simulated values (dashed curves) of extinction cross sections for two different configurations of layered slabs. The length $d = 26.82$ mm is chosen as the total length of configuration 2, *i.e.*, where the two dielectric slabs are separated by air. The theoretical curves are computed using lossless slabs with $\epsilon_{1r} = 2.1$ and $\epsilon_{2r} = 2.7$.

The resulting extinction cross sections are depicted in Figure 4, where the measured polarizabilities are $\gamma_1 = 3.14 \text{ cm}^3$ and $\gamma_2 = 3.13 \text{ cm}^3$ for the two configurations, respectively. The left hand side of (4.3) is estimated to 2.98 cm^3 and 2.94 cm^3 respectively for two cases, which shows that the right hand side and the left hand side of (4.3) are essentially the same for the two cases.

5.2 Array of lossy split ring resonators

Consider a quadratic split ring resonator (SRR) with unit cell length $\ell = 2.5$ mm. The design of the microstructure is similar to the split ring resonators discussed in [32]. The line width and distances in the SRR are $\ell/10$, see also [12] and Sec. 5.3. The SRRs are modeled as a resistive sheet having sheet resistance $R_s = 1/(\zeta d_0) = 1 \Omega$, where ζ and d_0 denote the bulk conductivity and thickness of the SRR [37]. The supporting dielectric structure is $d = 0.3$ mm thick and has the relative permittivity $\epsilon_r = 2$.

The transmission and reflection coefficients are simulated using CST Microwave Studio for $0.1 \text{ GHz} \leq f \leq 200 \text{ GHz}$. The absorption, σ_a , and scattering, σ_s , cross sections are determined from the transmission and reflection coefficients in analogy with (2.3) and (2.4), see Fig. 5. The extinction cross section is determined both as the sum $\sigma_{\text{ext}} = \sigma_a + \sigma_s$ and from the optical theorem (2.6), see Fig. 5.

The integrated extinction (4.3) is determined to $1.6\ell^3$, which is close to the low-frequency limit $\sigma_{\text{ext}}(k)/k \approx 1.7\ell^3$ for $k \approx 0$ and the polarizability $\gamma \approx 1.7\ell^3$ as determined using Comsol multiphysics, see also [12].

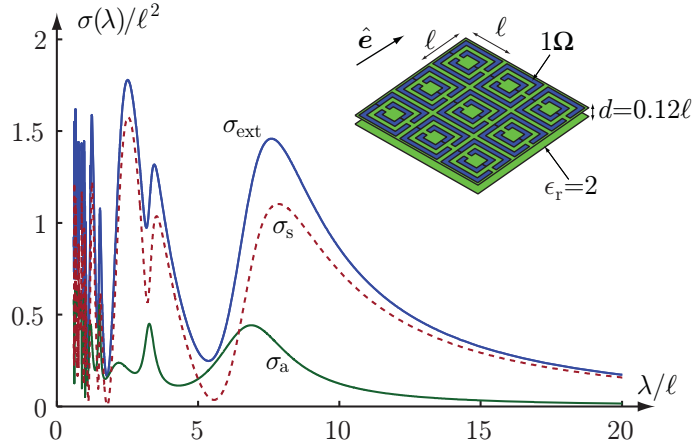


Figure 5: Simulated values for the absorption σ_a , scattering σ_s , and extinction σ_{ext} cross sections of an array of $1\ \Omega$ split ring resonators on a dielectric slab with $\epsilon_r = 2$ using CST.

5.3 Array of split ring resonators on a FR4 substrate

A finite periodic array of split ring resonators composed of 240×240 split ring resonators etched in $18\ \mu\text{m}$ thick copper and supported by a $0.6 \times 0.6\ \text{m}^2$ and $0.3\ \text{mm}$ thick dielectric substrate is used, see Fig. 6b. The experimental setup consists of a pair of wideband ridged horn antennas facing each other at a distance of $0.70\ \text{m}$ with the sample placed at the midpoint, see also [12]. The sample measurement is divided into two frequency intervals motivated by the necessity to use two different antenna pairs for the frequency bands $[1, 22]\ \text{GHz}$ and $[16, 40]\ \text{GHz}$. The sample measurement is normalized with a free space measurement and the resulting transmission coefficient is gated with a $2.3\ \text{ns}$ window in the time domain. The size of the window is chosen to minimize the influence of the background, and it reduces the useful frequency range to $[2.5, 38]\ \text{GHz}$.

The transmission coefficient is also determined numerically using the finite element solver in CST Microwave Studio for the horizontal and vertical polarizations. Since the sheet resistance of the copper layer is very low, $R_s = 1/(\zeta d) \approx 1\ \text{m}\Omega$, the copper is modeled as an infinitely thin perfect electric conductor, and the dielectric substrate is modeled with an isotropic temporally dispersive relative permittivity decreasing from 4.45 at $0.1\ \text{GHz}$ to 4.30 at $10\ \text{GHz}$. The overall loss factor is 0.02 according to the technical data sheet from the manufacturer. Fig. 6a depicts the real and imaginary parts of $h = i2A(1 - T)$, and the results from numerical simulations are in good agreement with the measured values.

The polarizability per unit area, $\hat{e} \cdot \gamma_e \cdot \hat{e}/A$, is estimated by solving (3.4) and (3.5) using the finite element solver from Comsol Multiphysics, where the static relative permittivity $\epsilon_r = 4.35$ is used. The result is $\hat{e} \cdot \gamma_e \cdot \hat{e}/A = 7.2\ \text{mm}$ and $\hat{e} \cdot \gamma_e \cdot \hat{e}/A = 7.1\ \text{mm}$ for the horizontal and vertical polarizations, respectively, see [12]. By numerically integrating the curves in Fig. 6, this integral is estimated to $6.3\ \text{mm}$ and $6.0\ \text{mm}$ for the horizontal and vertical polarizations, respectively. These values

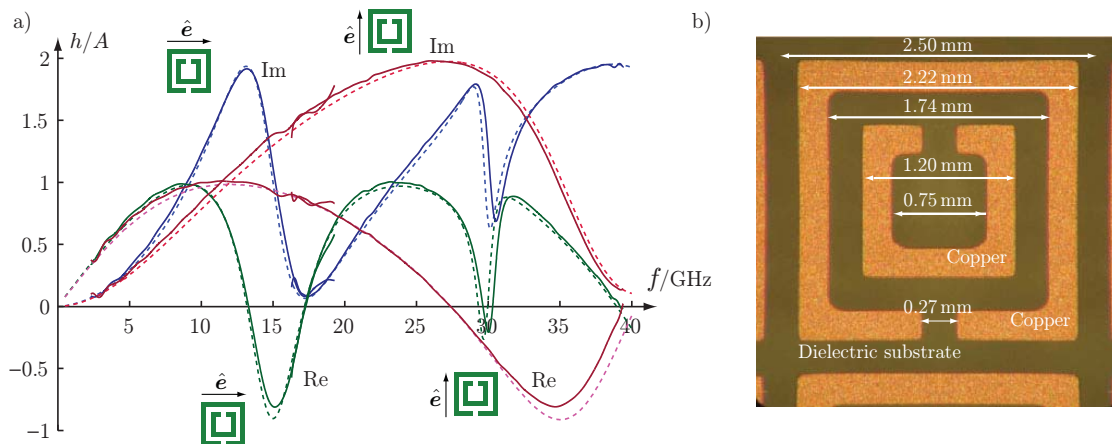


Figure 6: a) Measured values (solid curves) and simulated values (dashed curves) for the forward scattering of an array of split ring resonators on a FR4 substrate. b) Geometry of the split ring resonators on a 0.3mm thick FR4 substrate with $\epsilon_r = 4.35$.

are comparable with the right-hand side of (4.3) normalized by the cross section area of the unit cell. From (4.3) the slope of the real part at low frequencies is the static polarizability.

5.4 Resonant cylinder structure in a parallel plate waveguide

The forward scattering is determined for a set of SRRs on a cylindrical structure in a parallel plate waveguide [18]. The cylindrical structure is constructed by rolling up a $21.3 \times 63.9 \text{ mm}^2$ and 0.51 mm thick Arlon CLTE-XT sheet with 4×12 split ring resonators around an expanded polystyrene cylinder. The SRRs are etched in $18 \mu\text{m}$ thick copper as in Fig. 6b, but here with a unit cell length of $\ell = 5.32 \text{ mm}$ (the line width and distances are $\ell/10$) giving a resonance frequency around $f = 5 \text{ GHz}$. The outer radius of the cylinder is 10.2 mm. The experimental setup consists of a pair of TEM horn antennas facing each other at a distance 0.98 m with the sample placed in the center of the waveguide [18]. The sample measurement is normalized with a free space measurement [18]. The fluctuations at low frequencies in Fig. 7 are due to noise and interferences introduced in the measurement setup [18]. It is also noted that the setup is too small to use the time gating as used in the free space measurements in Fig. 6.

The forward scattered field is also determined numerically using the finite element solver in CST Microwave Studio as in Sec. 5.3 with the Arlon substrate modeled by the relative permittivity $\epsilon_r = 2.94$ and loss tangent 0.0025. The boundary conditions are modeled with periodic boundaries at the top and bottom of the cylinder and open boundaries for the other directions. It is observed that the numerical results resemble the measured values, see Fig. 7. The right hand side of (4.3) from simulations is calculated to 17.8 cm^3 which is the slope of the real part of the h function at low frequencies and the left hand side is estimated to 13 cm^3 over the frequency range

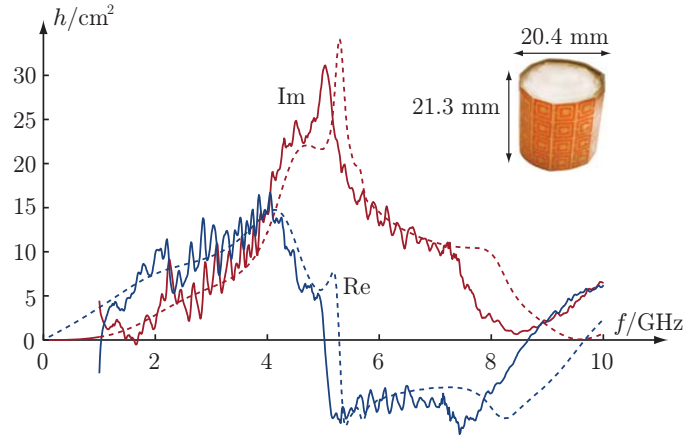


Figure 7: Measured values (solid curves) and simulated values (dashed curves) for the forward scattering of a resonant structure on an ARLON CLTE-XT substrate supported by an expanded polystyrene cylinder.

$f = [1 - 10]$ GHz. The measurement is noisy at low frequencies and not reliable to calculate the integral value in (4.3). Therefore the left hand side of sum rule is integrated from 2 GHz to 20 GHz and this value is estimated to 13.8 cm^3 . The measured values follow the simulated values and the areas under the $\sigma_{\text{ext}} = \text{Im } h$ curves are almost the same. The difference between the resonance frequencies is probably due to errors in the material modeling.

5.5 Periodicity in one direction

The one-dimensional periodic case in Fig. 2b and its corresponding sum rule is illustrated with the scattering of square PEC patches. The square patches have side lengths ℓ and are repeated periodically in the $\hat{\mathbf{x}}$ -direction with inter-element distances $\ell_x = n\ell$, for $n = 2, 5, 10, 20$. An in house method of moments (MoM) code is used to compute the forward scattering (4.7) for the incident wave $\mathbf{E}^{(i)}(\mathbf{r}) = \hat{\mathbf{e}} E_0 e^{ikz}$, see also App. A. The resulting extinction cross sections for the polarizations $\hat{\mathbf{e}} = \hat{\mathbf{x}}$ and $\hat{\mathbf{e}} = \hat{\mathbf{y}}$ are depicted in Fig. 8. The extinction cross sections $\sigma_{\text{ext},n}$ for the periodic structures ($n = 2, 5, 10, 20$) are compared with the extinction cross section for a single square patch ($n = \infty$).

The curves for $n = 10, 20, \infty$ are indistinguishable for the copolarized case, $\hat{\mathbf{e}} = \hat{\mathbf{x}}$, depicted in Fig. 8a illustrating that $\sigma_{\text{ext},n}$ approaches $\sigma_{\text{ext},\infty}$ fast as n increases. This fast convergence follows from the weak mutual coupling due to the null of the scattering pattern from the patches in the $\hat{\mathbf{e}} = \hat{\mathbf{x}}$ -direction. It is also observed that $\sigma_{\text{ext}} \approx 2\ell^2$ for short wavelength in agreement with the extinction paradox [26].

The convergence is much slower for the cross polarized case $\hat{\mathbf{e}} = \hat{\mathbf{y}}$ as depicted in Fig. 8b, where interference patterns are seen for inter-element distances equal to an integer number of wavelengths, *i.e.*, $n\ell = m\lambda$, $m = 1, 2, \dots$. This is similar to Wood's anomaly [13] and can be explained by the logarithmic singularity in the one dimensional periodic Green's function, see App. A. However, the influence of the

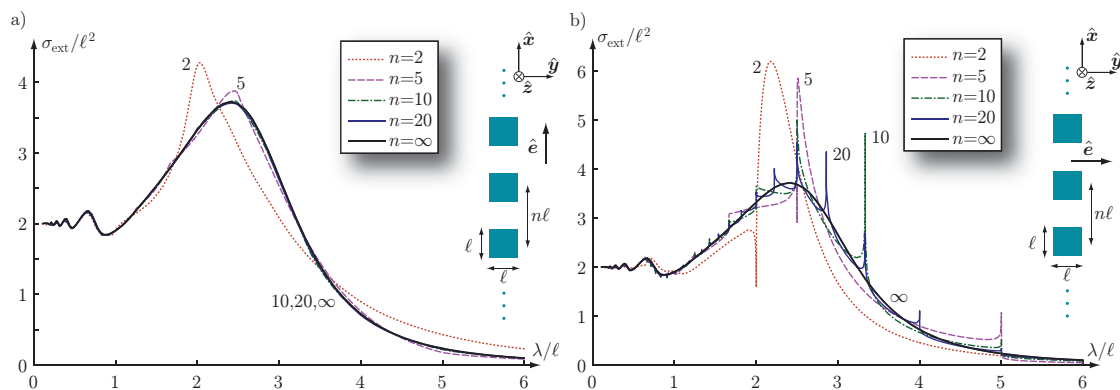


Figure 8: Extinction cross section for one dimensional repetitions of square PEC patches with side lengths ℓ and inter-element distances $n\ell$ for $n = 2, 5, 10, 20$. The incident field is $\mathbf{E}^{(i)} = E_0 \hat{e} e^{ikz}$ with $\lambda = 2\pi/k$. a) polarization $\hat{e} = \hat{x}$. b) polarization $\hat{e} = \hat{y}$.

singularities decay with the inter-element distance, $\ell_x = n\ell$, due to the division with ℓ_x in (A.2) and therefore $\sigma_{\text{ext},n}$ approaches $\sigma_{\text{ext},\infty}$ as $n \rightarrow \infty$.

The sum rule (4.3) is verified using MoM calculations for the electric polarizability dyadic giving $\gamma_e \approx (1.08\hat{x}\hat{x} + 1.00\hat{y}\hat{y})\ell^3$ for $n = 2$, $\gamma_e \approx (1.03\hat{x}\hat{x} + 1.02\hat{y}\hat{y})\ell^3$ for $n = 5$, and $\gamma_e \approx (1.03\hat{x}\hat{x} + 1.03\hat{y}\hat{y})\ell^3$ for $n = 10, 20$. There is no contribution from the magnetic polarizability dyadic in the \hat{z} direction. Numerical integrations of the left-hand side of the sum rule (4.3) over the finite range $\lambda/\ell \in [0.2, 30]$ give approximately 97% of the corresponding right-hand side.

6 Conclusions

We have presented an optical theorem for an arbitrary structure being periodic in a plane, which relates the extinction cross section per unit cell to the co-polarized transmission coefficient. For low pass structures this is used to derive a sum rule, which restricts the integral of the extinction cross section over all wavelengths by the static polarizability per unit cell. Sum rules for scatterers bounded in three and two dimensions (cylinders) are obtained as limits when the unit cell is taken to be very large in both or one directions, respectively. The theoretical results are shown to be in good agreement with numerical and experimental tests.

Acknowledgments

This work was supported in part by Swedish Research Council (VR) and the Swedish Foundation for Strategic Research (SSF).

Appendix A One dimensional periodic Green's functions

The free-space Green's function is $G = e^{ikR}/(4\pi R)$, where R denotes the distance between the source and observation point. Consider a one-dimensional periodic array in the $\hat{\mathbf{x}}$ -direction with inter-element distance ℓ_x . Here, we sum over all distances $R_n = ((x - x' - n\ell_x)^2 + (y - y')^2 + (z - z')^2)^{1/2}$ for integers n . The distance is asymptotically $R_n \sim |x - x' - n\ell_x|$ and $R_n^{-1} \sim 1/(|n|\ell_x)$ as $|n| \rightarrow \infty$. Use that

$$\sum_{n=1}^{\infty} \frac{e^{ik(n\ell_x + x' - x)}}{n\ell_x} = -\frac{e^{-ik(x-x')}}{\ell_x} \ln(1 - e^{ik\ell_x}) \quad (\text{A.1})$$

to rewrite the periodic Green's function as

$$G = \frac{e^{ikR_0}}{4\pi R_0} - 2 \frac{\cos(k(x-x'))}{4\pi\ell_x} \ln(1 - e^{ik\ell_x}) + \sum_{n \neq 0} \left(\frac{e^{ikR_n}}{4\pi R_n} - \frac{e^{ik|x-x'-n\ell_x|}}{4\pi|n|\ell_x} \right), \quad (\text{A.2})$$

where the logarithmic singularities for $k\ell_x = m2\pi$ or equivalently $\ell_x = m\lambda$, $m = 1, 2, \dots$ are observed.

References

- [1] A. Bernland, A. Luger, and M. Gustafsson. Sum rules and constraints on passive systems. *J. Phys. A: Math. Theor.*, **44**(14), 145205, 2011.
- [2] J. J. Bowman, T. B. A. Senior, and P. L. E. Uslenghi. *Electromagnetic and Acoustic Scattering by Simple Shapes*. North-Holland, Amsterdam, 1969.
- [3] F. Capolino, editor. *Theory and Phenomena of Metamaterials*. CRC Press, 2009.
- [4] R. M. Fano. Theoretical limitations on the broadband matching of arbitrary impedances. *Journal of the Franklin Institute*, **249**(1,2), 57–83 and 139–154, 1950.
- [5] M. Gustafsson. Sum rules for lossless antennas. *IET Microwaves, Antennas & Propagation*, **4**(4), 501–511, 2010.
- [6] M. Gustafsson. Time-domain approach to the forward scattering sum rule. *Proc. R. Soc. A*, **466**, 3579–3592, 2010.
- [7] M. Gustafsson, M. Cismasu, and S. Nordebo. Absorption efficiency and physical bounds on antennas. *International Journal of Antennas and Propagation*, (Article ID 946746), 1–7, 2010.
- [8] M. Gustafsson, C. Sohl, and G. Kristensson. Physical limitations on antennas of arbitrary shape. *Proc. R. Soc. A*, **463**, 2589–2607, 2007.

- [9] M. Gustafsson, C. Sohl, and G. Kristensson. Illustrations of new physical bounds on linearly polarized antennas. *IEEE Trans. Antennas Propagat.*, **57**(5), 1319–1327, May 2009.
- [10] M. Gustafsson. Sum rule for the transmission cross section of apertures in thin opaque screens. *Opt. Lett.*, **34**(13), 2003–2005, 2009.
- [11] M. Gustafsson and D. Sjöberg. Physical bounds and sum rules for high-impedance surfaces. *IEEE Trans. Antennas Propagat.*, **59**(6), 2196–2204, 2011.
- [12] M. Gustafsson, C. Sohl, C. Larsson, and D. Sjöberg. Physical bounds on the all-spectrum transmission through periodic arrays. *EPL Europhysics Letters*, **87**(3), 34002 (6pp), 2009.
- [13] A. Hessel and A. A. Oliner. A new theory of Wood’s anomalies on optical gratings. *Applied Optics*, **4**(10), 1275–1297, 1965.
- [14] J. D. Jackson. *Classical Electrodynamics*. John Wiley & Sons, New York, third edition, 1999.
- [15] D. S. Jones. Scattering by inhomogeneous dielectric particles. *Quart. J. Mech. Appl. Math.*, **38**, 135–155, 1985.
- [16] A. Karlsson. On the time domain version of the optical theorem. *Am. J. Phys*, **68**(4), 344–349, 2000.
- [17] R. E. Kleinman and T. B. A. Senior. Rayleigh scattering. In V. V. Varadan and V. K. Varadan, editors, *Low and high frequency asymptotics*, volume 2 of *Handbook on Acoustic, Electromagnetic and Elastic Wave Scattering*, chapter 1, pages 1–70. Elsevier Science Publishers, Amsterdam, 1986.
- [18] C. Larsson, S. E. Bayer, M. Gustafsson, G. Kristensson, D. Sjöberg, C. Sohl, and I. Vakili. Scattering measurements in a parallel plate waveguide – first results. In *Proceedings of the XXXth URSI General Assembly*, page B06.6, 2011.
- [19] D. Lytle, P. Carney, J. Schotland, and E. Wolf. Generalized optical theorem for reflection, transmission, and extinction of power for electromagnetic fields. *Phys. Rev. E*, **71**(5), 056610, 2005.
- [20] E. A. Marengo. A new theory of the generalized optical cross-section theorem for electromagnetic fields. In *Antennas and Propagation Society International Symposium, 2009. APSURSI’09. IEEE*, pages 1–4. IEEE.
- [21] B. Munk. *Frequency Selective Surfaces: Theory and Design*. John Wiley & Sons, New York, 2000.
- [22] R. Newton. Optical theorem and beyond. *Am. J. Phys*, **44**, 639–642, 1976.

- [23] A. M. Nicolson and G. F. Ross. Measurement of the intrinsic properties of materials by time-domain techniques. *IEEE Trans. Instrumentation and Measurement*, **19**, 377–382, 1970.
- [24] A. Nosich. Radiation conditions, limiting absorption principle, and general relations in open waveguide scattering. *Journal of electromagnetic waves and applications*, **8**(3), 329–353, 1994.
- [25] H. M. Nussenzveig. *Causality and dispersion relations*. Academic Press, London, 1972.
- [26] R. E. Peierls. *Surprises in Theoretical Physics*. Princeton University Press, 1979.
- [27] E. M. Purcell. On the absorption and emission of light by interstellar grains. *J. Astrophys.*, **158**, 433–440, 1969.
- [28] K. N. Rozanov. Ultimate thickness to bandwidth ratio of radar absorbers. *IEEE Trans. Antennas Propagat.*, **48**(8), 1230–1234, August 2000.
- [29] G. T. Ruck, D. E. Barrick, W. D. Stuart, and C. K. Krichbaum. *Radar Cross-Section Handbook*, volume 1 and 2. Plenum Press, New York, 1970.
- [30] D. Sjöberg. Low frequency scattering by passive periodic structures for oblique incidence: low pass case. *J. Phys. A: Math. Theor.*, **42**, 385402, 2009.
- [31] D. Sjöberg. Variational principles for the static electric and magnetic polarizabilities of anisotropic media with perfect electric conductor inclusions. *J. Phys. A: Math. Theor.*, **42**, 335403, 2009.
- [32] D. R. Smith, S. Schultz, P. Markos, and C. M. Soukoulis. Determination of effective permittivity and permeability of metamaterials from reflection and transmission coefficients. *Phys. Rev. B*, **65**, 195104–195108, 2002.
- [33] C. Sohl and M. Gustafsson. A priori estimates on the partial realized gain of Ultra-Wideband (UWB) antennas. *Quart. J. Mech. Appl. Math.*, **61**(3), 415–430, 2008.
- [34] C. Sohl, M. Gustafsson, and G. Kristensson. Physical limitations on broadband scattering by heterogeneous obstacles. *J. Phys. A: Math. Theor.*, **40**, 11165–11182, 2007.
- [35] C. Sohl, C. Larsson, M. Gustafsson, and G. Kristensson. A scattering and absorption identity for metamaterials: experimental results and comparison with theory. *J. Appl. Phys.*, **103**(5), 054906, 2008.
- [36] J. W. Strutt. On the light from the sky, its polarization and colour. *Phil. Mag.*, **41**, 107–120 and 274–279, April 1871. Also published in Lord Rayleigh, *Scientific Papers*, volume I, Cambridge University Press, Cambridge, 1899.

- [37] J. van Bladel. *Electromagnetic Fields*. IEEE Press, Piscataway, NJ, second edition, 2007.
- [38] W. B. Weir. Automatic measurement of complex dielectric constant and permeability at microwave frequencies. *Proc. IEEE*, **62**, 33–36, 1974.
- [39] H. Xu, D. Huber, and E. Heller. Cross section and optical theorem for defects on a corrugated surface. *The Journal of chemical physics*, **89**, 2550, 1988.
- [40] F. Yang and Y. Rahmat-Samii. *Electromagnetic band gap structures in antenna engineering*. Cambridge University Press, 2009.